INORGANIC CHEMISTRY
FRONTIERS

RESEARCH ARTICLE

View Article Online
View Journal | View Issue

Cite this: *Inorg. Chem. Front.*, 2025, **12**, 7863

Engineering solid-state structural transformations and reactions in complexes containing a natural alkaloid for specific switchable properties

Mia Mesić, [a] Marko Dunatov, [a] Andreas Puškarić, [a] Glorija Medak, [a] Robert Kruk [b] and Lidija Androš Dubraja *[a]

Molecule-based crystals that respond to environmental stimuli such as light, temperature, pressure, electricity and humidity are attractive candidates for smart materials, *i.e.* sensors, actuators, optoelectronic devices, information storage, medical applications, *etc*. The design strategies for stimuli-responsive molecular materials are based on the interplay between weaker intermolecular interactions and flexible constituent units, *e.g.* pseudo-spherical organic cations and halogenometalate anions. In this context, solid-state structural transformations of a metal complex containing a natural alkaloid with a quasi-spherical fragment, the cinchoninium–trichloro–cobalt(II), were investigated under the influence of various stimuli. The cinchoninium-trichloro-cobalt(II) complex was dynamically modified post-synthetically by exposing it to (i) different small molecules in the vapour phase (water, methanol, acetonitrile, hydrochloric acid) or (ii) grinding conditions with small molecules (mechanochemical reaction), resulting in six different crystal phases. The structural transformations, their reversibility and selectivity towards small molecules were investigated by a combination of vacuum infrared spectroscopy and powder X-ray diffraction methods, supported by single-crystal X-ray diffraction analysis. The study of the effects of exposure to solvent molecules either in the vapour phase or by post-synthetic grinding on the crystal structure of the final product provided insights into the control of crystallographic symmetry (enhancement or breaking) and an understanding of the origin of the resistive sensing and static magnetic properties in the cinchonine–chloro–cobalt(II) system.

Received 6th May 2025,
Accepted 21st August 2025

DOI: 10.1039/d5qi01084e

rsc.li/frontiers-inorganic

Introduction

The ability of crystalline solids to change reversibly under the influence of external stimuli, such as electrical, magnetic, chemical and thermal stimuli, is important for the development of new devices and technologies, particularly for applications in the fields of (bio)sensors, actuators, information storage, optoelectronics, spintronics and medical treatment.[1–4] In this context, molecule-based materials are the most promising candidates to exhibit the stimuli-responsive behaviour, mainly due to the soft crystal packing mediated by intermolecular interactions, which favours structural transformations with a lower energy barrier.[5–7] The study of these crystalline materials at the molecular level could contribute to a better understanding of the specific stimuli-responsive behaviour and lead to the development of materials for applications such as ferroelectrics, sensors and switchable dielectric devices.[8–10] Molecular and crystal engineering offers numerous possibilities for designing molecular materials, based primarily on coordination chemistry and organic ligand synthesis.[11] Multifunctional organic ligands with several donor and acceptor sites are common structural motifs which, in combination with specific metal ions and various counter ions can lead to the formation of either discrete molecular-based compounds or structures with extended architectures such as coordination polymers.[12] However, when considering only the principles of chemical synthesis, predicting the outcome of chemical reactions is often difficult. For a better understanding of product formation, it is important to account not only for the coordination bonds formed by such complexes but also for the prediction of weaker intermolecular interactions.[13,14] In the search for suitable organic ligands for the synthesis of stimuli-responsive materials, it is logical to look for inspiration in naturally occurring compounds.[15] *Cinchona* alkaloids, *e.g.* quinine and cinchonine, are easily accessible natural chiral compounds that can be extracted from the bark of *Cinchona pubescens*.[16] Their structure contains the quinoline ring, which

[a]*Ruđer Bošković Institute, Bijenička cesta 54, 10000 Zagreb, Croatia. E-mail: lidija.andros@irb.hr; Tel: +385 1 4561184*
[b]*Institute of Nanotechnology, Karlsruhe Institute of Technology, Hermann-von-Helmholtz-Platz 1, 76344, Eggenstein-Leopoldshafen, Germany*

provides the possibility of making stacking interactions, and quasi-spherical polar quinuclidine fragment, which is well known for its low energy rotational properties.[17] The *Cinchona* alkaloids and their derivatives have been intensively studied from the point of view of medicinal applications,[18] enantioselective catalysis and separation,[19] and as chiral building blocks for metal–organic supramolecular architectures.[20,21] To develop functional materials based on *Cinchona* alkaloids, it is necessary to understand, at the molecular level, the supramolecular forces that govern the self-assembly of the associated complexes. The crystal structure provides the best insight into these forces.[22,23] In this work, the structural transformations of a cinchoninium–trichloro–cobalt(II) complex, [(H–Cn)$CoCl_3$], (cinchoninium, H–Cn = $C_{19}H_{23}N_2O$) with polar $P2_1$ structure were investigated using two different post-synthetic approaches. In the first approach, the starting phase [(H–Cn)$CoCl_3$] was exposed to solvent vapours to induce structural changes, and in the second approach it was modified mechanochemically. The formation and stability of different cinchonine–chloro–cobalt(II) compounds were discussed in the context of their crystal structures and intermolecular interactions. The structural changes were monitored *in situ* by infrared spectroscopy in vacuum and powder X-ray diffraction. The influence of structural changes on magnetic and electrical (sensing) properties was discussed.

Experimental

Materials

Cinchoninium chloride dihydrate (85%), (H–Cn)Cl·$2H_2O$, was purchased from Sigma Aldrich and cobalt(II) chloride hexahydrate (98%), $CoCl_2·6H_2O$, was purchased from Alfa Aesar. Methanol and acetonitrile were purchased from J. T. Baker and ethanol was purchased from Gram-mol (w = 97%). Concentrated hydrochloric acid was purchased from BDH Aristar Plus (w = 35%).

Synthesis of [(H–Cn)$CoCl_3$]

(H–Cn)Cl·$2H_2O$ (m = 92 mg; n = 0.25 mmol) and $CoCl_2·6H_2O$ (m = 119 mg; n = 0.5 mmol) were dissolved in a mixture of ethanol and diethyl–ether. Blue prism-like single crystals of cinchoninium–trichloro–cobalt(II) complex, [(H–Cn)$CoCl_3$], formed within a day. Anal. calcd % for $C_{19}H_{23}N_2OCoCl_3$ (found, %): C, 49.53 (49.75); H, 5.03 (5.52); N, 6.08 (6.22); Co, 12.79 (12.96); Cl, 23.08 (23.58).

Crystallographic measurements

The single-crystal X-ray diffraction data for [(H–Cn)$CoCl_3$], [(H–Cn)$CoCl_3$]·CH_3OH, [H_2–Cn][$CoCl_4$] and [H_2–Cn][$CoCl_4$]·CH_3CN were collected by ω-scans using Cu-Kα radiation (λ = 1.54179 Å, microfocus tube, mirror monochromator) using a Rigaku XtaLAB Synergy diffractometer at 293 K. The crystal data, experimental conditions and the final refinement parameters are summarized in Table S1 in the SI. Data reduction, including the multiscan absorption correction, was performed using the CrysAlisPRO software package. The molecular and crystal structures were solved by direct methods using the program SIR2019[24] and refined by the full-matrix least-squares method based on F^2 with anisotropic displacement parameters for all non-hydrogen atoms (SHELXL-2014/7).[25] Both programs were operating under the WinGX program package.[26] Hydrogen atoms attached to the C atoms were treated as riding in idealized positions, with the C–H distances of 0.97 or 0.93 Å and displacement parameters assigned as $U_{iso}(H) = 1.2U_{eq}(C)$. Hydrogen atoms of hydroxyl group and protonated nitrogen were identified based on different Fourier maps and distances of O–H and N–H bonds were restrained. Geometrical calculations were carried out using PLATON[27] and the figures were generated using CCDC-Mercury[28] programs. Dipole moment calculations were performed with semi-empirical quantum chemistry method ZINDO implemented in ArgusLab program.[29] The powder X-ray diffraction (PXRD) data were collected in reflection mode using Cu-Kα radiation (λ = 1.54060 Å) using a Malvern Panalytical Empyrean diffractometer with a step size of 0.013° in a 2θ range between 4° and 50°. The peak search and indexing for phases [(H–Cn)$CoCl_3$]·H_2O, [H_2–Cn][$CoCl_4$]·CH_3OH and [H_2–Cn][$CoCl_4$]·H_2O were carried out using the TOPAS software. Unit cell and profile refinements were carried out using the Pawley method.[30] Crystallographic data, structure refinement details with profile fitting of the PXRD data are given in Table S2 and Fig. S1 in the SI. Crystallographic parameters for all crystal phases are given in Table 1.

Thermal analysis

Thermogravimetric analysis (TG) were carried out in a Shimadzu DTG-60H analyser at a rate of 10 K min^{-1} from 300 K to 973 K under a flow of dry air.

Spectroscopic measurements

Fourier transformed infrared (FTIR) spectra were recorded in the 4000–400 cm^{-1} range using a PerkinElmer FTIR Frontier spectrometer, in the transmission mode under ambient pressure, reduced pressure of 1×10^{-3} mbar and during exposure to 25–100 ppm of probe molecule at reduced pressure. The samples were diluted for transmission mode by preparing a thin film of the sample (drop-casting of the methanol solution) on the NaCl pastille.

Electrical and magnetic measurements

The current response during exposure to methanol vapours was monitored by chronoamperometric measurements with a PalmSens4 potentiostat. For measurements the polycrystalline sample was pressed into a cylindrical pellet with a diameter of 5 mm and a thickness of 0.5 mm having 3.5 mm diameter sputter coated Au electrodes on the opposite surfaces of the pellet. The temperature dependence of the magnetic susceptibility in the range of 2–293 K in a field of 1000 Oe was measured with a Quantum Design MPMS-3 magnetometer equipped with a superconducting quantum interferometer device.

Table 1 Unit cell parameters and space group of the various cinchonine–chloro–cobalt(II) complexes and complex salts

Compound	[(H–Cn)$CoCl_3$]	[(H–Cn)$CoCl_3$]·CH_3OH	[(H–Cn)$CoCl_3$]·H_2O	[H_2–Cn][$CoCl_4$]	[H_2–Cn][$CoCl_4$]·CH_3OH	[H_2–Cn][$CoCl_4$]·H_2O	[H_2–Cn][$CoCl_4$]·CH_3CN
Formula	$C_{19}H_{23}Cl_3CoN_2O$	$C_{20}H_{27}Cl_3CoN_2O_2$	$C_{19}H_{25}Cl_3CoN_2O_2$	$C_{19}H_{24}Cl_4CoN_2O$	$C_{20}H_{28}Cl_4CoN_2O_2$	$C_{19}H_{26}Cl_4CoN_2O_2$	$C_{21}H_{27}Cl_4CoN_3O$
M_r/g mol^{-1}	460.67	492.71	478.70	497.13	529.19	515.16	538.18
Crystal system	Monoclinic	Monoclinic	Monoclinic	Orthorhombic	Orthorhombic	Orthorhombic	Orthorhombic
Space group	$P2_1$	$P2_1$	$P2_1$	$P2_12_12_1$	$P2_12_12_1$	$P2_12_12_1$	$P2_12_12_1$
a/Å	8.414	9.263	8.573	7.024	32.585	12.663	8.839
b/Å	12.741	12.948	13.051	15.007	8.865	13.371	11.884
c/Å	10.054	9.305	9.916	21.172	8.234	25.604	23.988
α/°	90	90	90	90	90	90	90
β/°	97.46	93.06	96.94	90	90	90	90
γ/°	90	90	90	90	90	90	90
Z	2	2	2	4	4	4	4
V/Å^3	1068.86	1114.56	1101.43	2231.92	2378.81	4335.63	2520.0

Results and discussion

Screening for crystal transformations

In general, the metal complexes of *Cinchona* alkaloids as homochiral building blocks are suitable candidates for the construction of polar supramolecular architectures in the solid state.[20–23] The chemical and thermal stability of *Cinchona* alkaloids makes them excellent and inexpensive chelating ligands for the construction of chiral metal complexes and networks, which is of potential interest for developing new materials for nonlinear optics, piezoelectrics and ferroelectrics. The cations of the *Cinchona* family consist of quinoline rings, which provide stability through possible aromatic interactions, and quinuclidine fragments, which offer flexibility through low-energy rotational flexibilitiy.[17] Both the quinoline and quinuclidine nitrogen atoms can be protonated, so the *Cinchona* alkaloids can occur as mono- or dications. Given the above-mentioned structural adaptability and the manifold possibilities of intermolecular interactions offered by *Cinchona* alkaloids, it should be investigated how the structure and properties of the *Cinchona* alkaloid-metal complex in the solid state can be altered by gentle external stimuli (*e.g.* above room temperature heating, vacuum conditions, exposure to small molecules). For this purpose, a solvent-free cinchoninium–trichloro–cobalt(II) complex, [(H–Cn)$CoCl_3$], was prepared as a starting phase, which was exposed to solvent vapours (water, methanol, acetonitrile, hydrochloric acid), and mechanochemical reactions with solvents to induce structural transformations in the solid state and possibly lead to switchable properties. The starting [(H–Cn)$CoCl_3$] phase is a neutral complex in which cobalt(II) adopts a tetrahedral geometry consisting of three chlorine atoms and one nitrogen atom of the quinoline ring, while the quinuclidine nitrogen of cinchonine is protonated. According to PXRD measurements (Fig. 1), exposure of the [(H–Cn)$CoCl_3$] compound to methanol vapours induces structural changes, resulting in the formation of a new phase that incorporates methanol and is referred to here as [(H–Cn)$CoCl_3$]·CH_3OH. This structural and compositional change is reversible, and the initial solvent-free phase [(H–Cn)$CoCl_3$] can be obtained either by heating [(H–Cn)$CoCl_3$]·CH_3OH to 400 K (Fig. S5 in the SI) or by exposure to vacuum conditions.

To further test the affinity of other molecules for incorporation into the crystal structure of [(H–Cn)$CoCl_3$], two proton molecule (H_2O), a polar aprotic solvent (CH_3CN) and a strongly acidic molecule (HCl) were introduced to [(H–Cn)$CoCl_3$] in the vapour phase. The investigations revealed that the energy barrier for water molecules transitioning from the gas phase into the solid-state structure of [(H–Cn)$CoCl_3$] is too high for this process to occur under humid atmospheric conditions. After exposing the compound to air with a relative humidity of more than 90%, no structural change occurs. However, the aqueous phase of the compound, [(H–Cn)$CoCl_3$]·H_2O, can be obtained directly mechanochemically using the starting reactants [(H–Cn)$CoCl_3$] and H_2O (see Fig. 1, sample c). Acetonitrile, on the other hand, has no effect on the [(H–Cn)$CoCl_3$] compound, neither by exposing [(H–Cn)$CoCl_3$] to the

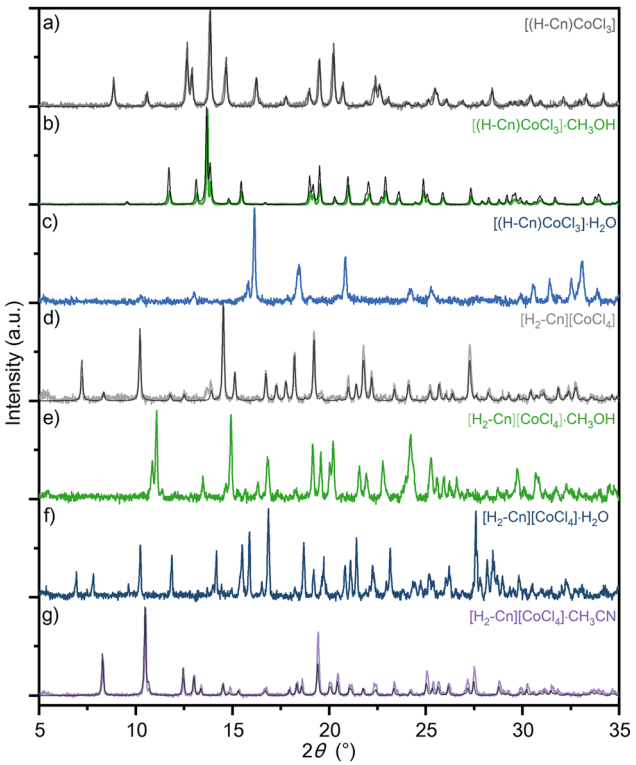

Fig. 1 PXRD patterns of various cinchonine–chloro–cobalt(II) complexes prepared by solid-state transformation. The experimental data are confirmed by calculated PXRD patterns from single-crystal XRD data (black lines).

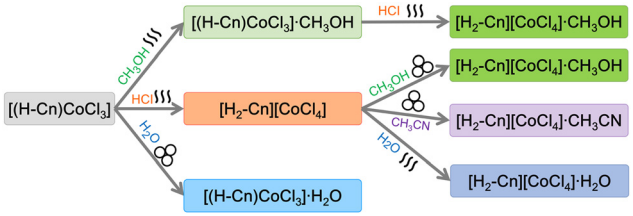

Scheme 1 Different phases in the cinchonine–chloro–cobalt(II) system obtained from the starting compound [(H–Cn)$CoCl_3$] upon reaction with small molecules either by exposure to vapours or by mechanochemical processes.

CH_3CN vapour phase at atmospheric conditions nor by mechanochemical reaction of [(H–Cn)$CoCl_3$] with CH_3CN. The corrosive hydrochloric acid vapours are very reactive and lead to the reconstructive solid-state transformation.[31] The starting cinchonine–trichloro–cobalt(II) complex is decomposed and a complex salt [H_2–Cn][$CoCl_4$] is formed by protonation of the quinoline nitrogen of the cinchonine molecule and introduction of additional chlorine into the coordination sphere of cobalt(II) (see Fig. 1, pattern d). The structure of a complex salt [H_2–Cn][$CoCl_4$] is also subject to changes mediated by the presence of small molecules. The complex salt [H_2–Cn][$CoCl_4$] has its own selectivity towards small molecules, which differs from that of a discrete complex compound [(H–Cn)$CoCl_3$]. Water molecules from humid air cause a structural change leading to the hydrate phase of the complex salt [H_2–Cn][$CoCl_4$]·H_2O (Fig. 1, pattern f). The presence of methanol or acetonitrile in the vapour phase has no effect on the structure of [H_2–Cn][$CoCl_4$], but with an energetic stimulus from a mechanochemical reaction, these molecules can penetrate the material structure to give the solvate phases [H_2–Cn][$CoCl_4$]·CH_3OH (Fig. 1, pattern e) and [H_2–Cn][$CoCl_4$]·CH_3CN (Fig. 1, pattern g). Scheme 1 summarizes the described processes, where it was found from the PXRD analysis that two different phases can be obtained from the initial [(H–Cn)$CoCl_3$] complex by exposing it to small molecules in the vapour phase, and that another phase can be isolated by the mechanochemical reaction. Further on, the newly formed phase [H_2–Cn][$CoCl_4$] undergoes mechanochemical post-synthetic modification to methanol and acetonitrile solvate, while water molecules are able to enter the structure from air humidity.

The TG analysis (Fig. S5 and Table S7 in the SI) shows that the compound [(H–Cn)$CoCl_3$] is stable up to 500 K. Methanol starts to eliminate from the compound [(H–Cn)$CoCl_3$]·CH_3OH at 340 K and the process is over at 400 K. The compound [(H–Cn)$CoCl_3$]·H_2O is very unstable and the water molecule is already eliminated in presence of dry air. For the complex salts [H_2–Cn][$CoCl_4$]·CH_3OH and [H_2–Cn][$CoCl_4$]·CH_3CN, the elimination of the solvent molecules starts at ~340 K and ends at ~400 K. The TG analysis shows that the hydrate complex salt is more stable than the hydrate complex, which is consistent with other measurements.

Crystal structures

The observed structural changes as well as the selectivity of the uptake of individual solvent molecules are observed by detailed structural studies of the crystal packing. The crystal structures were solved based on single-crystal X-ray diffraction data for the phases [(H–Cn)$CoCl_3$], [(H–Cn)$CoCl_3$]·CH_3OH, [H_2–Cn][$CoCl_4$] and [H_2–Cn][$CoCl_4$]·CH_3CN. For the [(H–Cn)$CoCl_3$]·H_2O, [H_2–Cn][$CoCl_4$]·H_2O and [H_2–Cn][$CoCl_4$]·CH_3OH phases, the unit cell parameters and the space group were determined by indexing the PXRD data (Fig. S1 in the SI). Table 1 contains the unit cell parameters for all isolated phases in the cinchonine–chloro–cobalt(II) system. Asymmetric units for the compounds [(H–Cn)$CoCl_3$], [(H–Cn)$CoCl_3$]·CH_3OH, [H_2–Cn][$CoCl_4$] and [H_2–Cn][$CoCl_4$]·CH_3CN are shown in Fig. 2, and the geometrical parameters describing the cobalt(II) coordination sphere are given in Table S3 in the SI. In the [(H–Cn)$CoCl_3$] and [(H–Cn)$CoCl_3$]·CH_3OH complexes, cobalt(II) adopts a tetrahedral geometry consisting of three chlorine atoms and one nitrogen atom of the quinoline ring. In the [H_2–Cn][$CoCl_4$] and [H_2–Cn][$CoCl_4$]·CH_3CN phases, both nitrogen atoms of the cinchonine molecule are protonated, and cobalt(II) adopts an almost regular tetrahedral geometry with four chlorine atoms. The distances between the Co–Cl bonds are fairly uniform and ranging from 2.234 to 2.296 Å (Table S3 in the SI). As expected, the deviation from the ideal tetrahedral geometry is larger for the [(H–Cn)$CoCl_3$] and

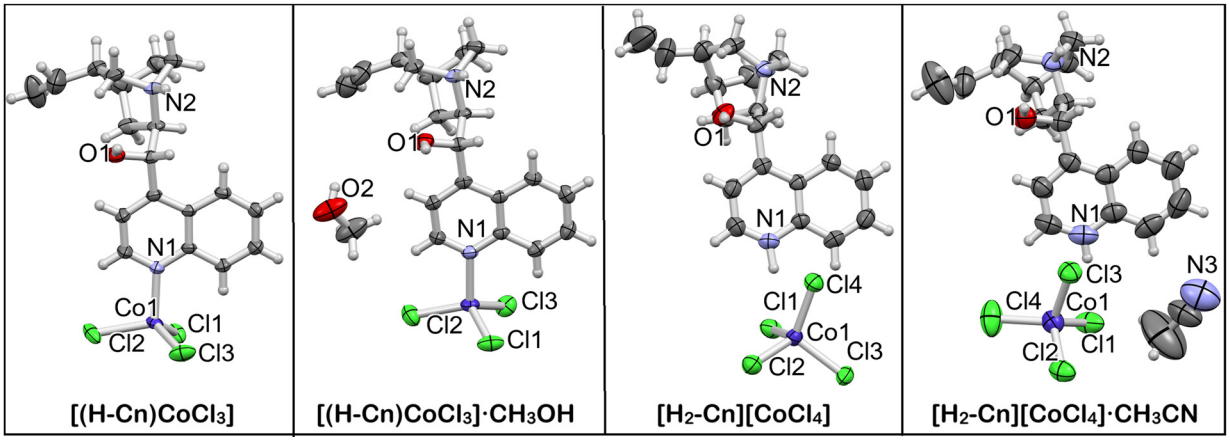

Fig. 2 ORTEP-3 drawings of the compounds [(H–Cn)$CoCl_3$], [(H–Cn)$CoCl_3$]·CH_3OH, [H_2–Cn][$CoCl_4$] and [H_2–Cn][$CoCl_4$]·CH_3CN, showing displacement ellipsoids for the probability of 50% and hydrogen atoms as spheres of arbitrary radius, including atom numbering scheme for non-C, H atoms.

[(H–Cn)$CoCl_3$]·CH_3OH complexes due to the coordinated cinchonine molecule, *i.e.* the presence of the Co–N bond.

The initial [(H–Cn)$CoCl_3$] complex crystallizes in the polar monoclinic space group $P2_1$ (Table 1).[32] There are two main intramolecular contacts that stabilize the three-dimensional supramolecular architecture: first, hydrogen bonds between the hydrogen on the hydroxyl group and a chlorine atom and the second one is between the hydrogens attached to the quinuclidine nitrogen and the chlorine atom, which propagate along the [001] direction (Fig. 3a); and second, the C–H···π type aromatic interaction, which runs along the [100] direction. Details of the hydrogen bonds and aromatic stacking geometry can be found in Tables S4–S6 in the SI. The incorporation of a methanol molecule leads to the formation of the methanol solvate [(H–Cn)$CoCl_3$]·CH_3OH, which also has the polar $P2_1$ structure. With the entry of methanol into the structure, the strongest intermolecular contact becomes the one between the methanol and the neutral unit of the complex, *i.e.* the methanol molecule serves as a mediator in the formation of an infinite one-dimensional hydrogen bond in the [001] direction (Fig. 3b). According to the analysis of the contact surface void analysis in program Mercury,[28] the compound [(H–Cn)$CoCl_3$] contains a free volume of 49 $Å^3$ in the structure (green coloured areas in Fig. 3a). The contact surface void of methanol in the structure of [(H–Cn)$CoCl_3$]·CH_3OH is about 96 $Å^3$, indicating that only a small change in the volume of the unit cell is required to accommodate one methanol molecule (see Table 1). The presence of corrosive hydrochloric acid vapours leads to the dissociation of the neutral [(H–Cn)$CoCl_3$] complex compound in the solid state, whereby the coordination sphere of cobalt(II) changes due to the coordination of an additional chlorine atom and the quinoline nitrogen is simultaneously protonated, resulting in a complex salt [H_2–Cn][$CoCl_4$]. This structural change leads to an increase in the symmetry of the system from monoclinic $P2_1$ to orthorhombic $P2_12_12_1$, whereby the polar structure is lost.[23,32] Closer examination of the crystal structures shows that the nitrogen atom of the quinoline ring, which forms a coordinative bond of 2.057 Å with the cobalt in [(H–Cn)$CoCl_3$], moves away by about 2 Å with respect to the cobalt atom in the [H_2–Cn][$CoCl_4$]

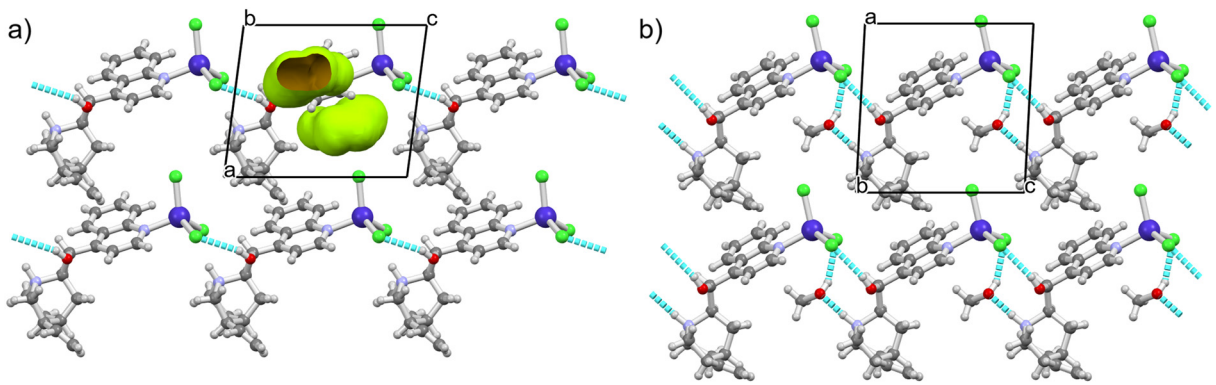

Fig. 3 One-dimensional hydrogen bond chains along the [001] direction in: (a) [(H–Cn)$CoCl_3$] (green areas represent the free volume); (b) [(H–Cn)$CoCl_3$]·CH_3OH. Hydrogen contacts are shown as cyan-coloured rods.

complex salt (to a total distance Co···N of 4.053 Å), creating a hydrogen bond between the now protonated quinoline nitrogen and the chlorine coordinated to the cobalt. During the transformation, the cobalt atoms move apart in the direction of the *c*-axis and move closer in the direction of the *a*-axis by about 1.4 Å (see Fig. 4).

Comparing the crystal packing features of [(H–Cn)$CoCl_3$] and [H_2–Cn][$CoCl_4$], the C–H···π type contacts in [(H–Cn)$CoCl_3$] are replaced by Co–Cl···π type of contacts (the geometry of the contacts is given in Table S5 in the SI). One-dimensional hydrogen bonds in [(H–Cn)$CoCl_3$] propagate along the *c*-axis, while in [H_2–Cn][$CoCl_4$] stronger H-bond contacts are formed in the *ac*-plane.

The acetonitrile solvate [H_2–Cn][$CoCl_4$]·CH_3CN also crystallizes in the orthorhombic space group $P2_12_12_1$, confirming that the polarity of the structure is primarily related to the loss of the dipole moment of the anion associated with the change in the cobalt(II) coordination sphere when the nitrogen donor atom is replaced by chlorine. Acetonitrile as a molecule with a large dipole moment (5.5 D in the acetonitrile crystal)[33] has no influence on the restoration of the polar crystal structure.

Compared to the solvent-free structure, intermolecular contacts in the acetonitrile solvate are energetically weaker, and the solvent molecule can be easily removed from the structure either by heating or under vacuum conditions. However, neither acetonitrile nor methanol from the solvent vapour can penetrate the [H_2–Cn][$CoCl_4$] structure, unlike in the mechanochemical reaction, where additional energy input enables such structural changes.

Spectroscopic characterization

To gain insight into the dynamics of the crystal transformation process in cinchonine–chloro–cobalt(II) compounds and the selectivity for certain small molecules, *in situ* FTIR measurements were performed in transmission mode at reduced pressure and controlled atmosphere. The first spectra of the compound [(H–Cn)$CoCl_3$]·CH_3OH was recorded at atmospheric pressure. The reduced pressure (1×10^{-3} mbar) caused the elimination of the methanol molecule and the formation of the solvent-free [(H–Cn)$CoCl_3$] phase (see Fig. S3 in the SI). After the addition of 25 ppm methanol to the closed system of the vacuum FTIR cell, a conversion to the methanol phase [(H–Cn)$CoCl_3$]·CH_3OH occurred almost immediately (Fig. 5a). This

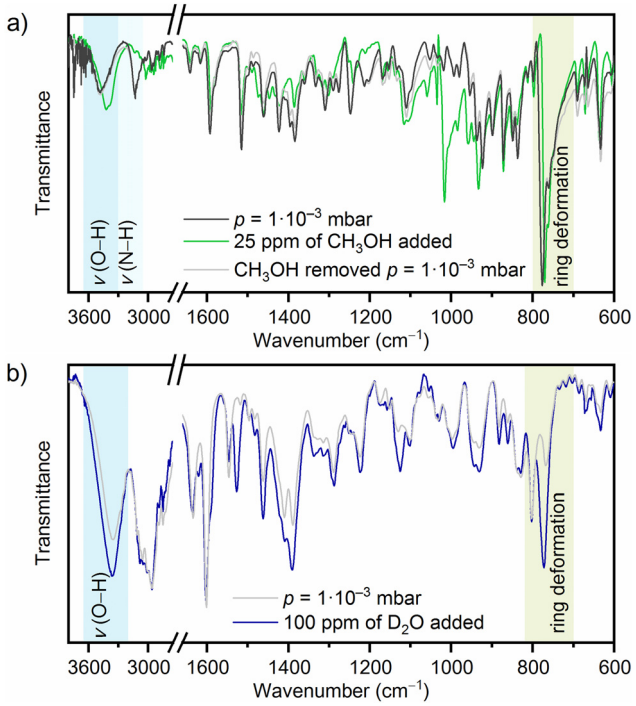

Fig. 5 Vacuum FTIR observation of structural transformation: (a) in the solvent-free phase [(H–Cn)$CoCl_3$] during exposure and subsequent removal of methanol; (b) in the solvent-free phase [H_2–Cn][$CoCl_4$] during exposure and subsequent removal of D_2O.

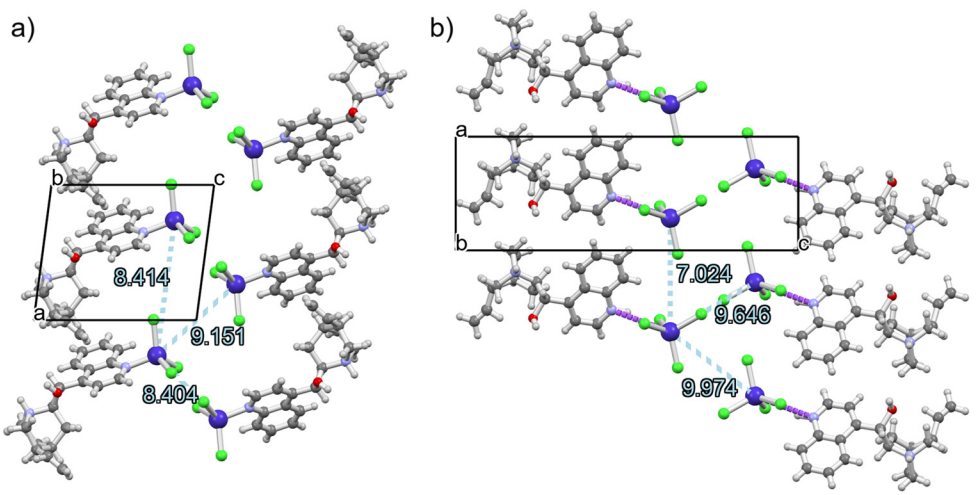

Fig. 4 Change in crystal packing during the transformation of (a) [(H–Cn)$CoCl_3$] complex to (b) [H_2–Cn][$CoCl_4$] complex salt obtained by the exposure to HCl vapours. The Co–N contacts are shown as violet rods. The distances between the cobalt atoms are given in Å.

structural transformation can be recognized by two major spectral changes: bands at 3480 and 3127 cm^{-1}, which are associated with the ν(O–H) and ν(N–H) stretching vibrations of the hydrogen atoms of the hydroxyl group and the protonated quinuclidine nitrogen,[34] respectively, shift to lower wavenumbers as methanol reduces the freedom of movement of these bonds. Together with the small shifts in position of the weaker bands, the most intense band in the spectra associated with the ring deformation of the quinoline group also shifts to lower frequencies from 776 cm^{-1} to 770 cm^{-1}.[35] Performing the same experiment with the addition of the deuterated solvents CD_3CN and D_2O (2 h exposure at 100 ppm) had no effect on the spectra of the initial solvent-free phase [(H–Cn)$CoCl_3$], which is consistent with the PXRD measurements showing that water enters this system only by a mechanochemical reaction and acetonitrile does not enter at all.

The complex salt systems show different behaviour in the presence of small molecules in the vapour phase. First, the FTIR spectra were recorded at atmospheric conditions for the methanol phase [H_2–Cn][$CoCl_4$]·CH_3OH. Reducing the pressure led to the elimination of the methanol molecule and the formation of the solvent-free phase [H_2–Cn][$CoCl_4$] (Fig. S4 in the SI). After the addition of 100 ppm D_2O to the closed system of the vacuum FTIR cell, the conversion to the hydrate phase [H_2–Cn][$CoCl_4$]·D_2O occurred (Fig. 5b), recognizable by a new broad band at 2222 cm^{-1} related to the stretching vibration of ν(O–D).[36] In addition, a ν(O–H) stretching vibrations associated with the hydrogen atoms of the hydroxyl group of cinchonine centred at 3350 cm^{-1}, shifts to 3360 cm^{-1} and increase in intensity. The presence of water molecules in the structure is also reflected in a change in the position and intensity of the band related to the deformation of the quinoline ring at 768 cm^{-1}, which is due to pronounced stacking interactions that are quite suppressed in [H_2–Cn][$CoCl_4$].[35] The addition of water obviously weakens the stacking interactions and the vibrations related to ring deformation increase, and the band related to these vibrations increases in intensity and shifts to higher frequencies at 772 cm^{-1}. Performing the same experiment with the addition of methanol and acetonitrile (2 h exposure at 100 ppm) had no effect on the spectra of the initial solvent-free [H_2–Cn][$CoCl_4$], showing that these molecules can only enter the structure through a mechanochemical reaction and not from the vapour phase.

Static magnetic properties

The dc magnetic susceptibility at variable temperature was measured on powdered crystalline samples of [(H–Cn)$CoCl_3$]·CH_3OH and [H_2–Cn][$CoCl_4$] phase at a field of 1000 Oe over the temperature range of 2–293 K (Fig. 6). The calculated magnetic susceptibility values show a paramagnetic behaviour as expected for mononuclear cobalt(II) complexes with S = 3/2. At room temperature, the $\chi_M T$ product is 2.86 cm^3 K mol^{-1} for [(H–Cn)$CoCl_3$]·CH_3OH, and 2.64 cm^3 K mol^{-1} for [H_2–Cn][$CoCl_4$]. For both compounds, the $\chi_M T$ value remains approximately constant from room temperature to 100 K before decreasing slightly. This temperature profile is consistent with the Curie behaviour for non-interacting mononuclear Co(II) centres, while the observed decrease below 100 K is most likely due to the intrinsic magnetic anisotropy of the Co(II) ions. For the complex salt [H_2–Cn][$CoCl_4$], the $\chi_M T$ product decreases with decreasing temperature below 100 K and reaches a value of 2.07 cm^3 K mol^{-1} at 2.5 K. For the [(H–Cn)$CoCl_3$]·CH_3OH complex, the $\chi_M T$ value decreases to 2.63 cm^3 K mol^{-1} at 14 K and then increases rapidly to reach a maximum of 2.90 cm^3 K mo1^{-1} at 8 K, followed by a rapid decrease to 2.05 cm^3 K mol^{-1} at 2.5 K. This increase at low temperatures is probably related to intermolecular ferromagnetic interactions, which can be explained by closer inspection of the [(H–Cn)$CoCl_3$]·CH_3OH crystal packing. Although the metal centres are far apart (Co···Co is 9.263 Å), the two molecules of the [(H–Cn)$CoCl_3$] complex are linked by a strong hydrogen bond propagating along the [100] direction, in which the hydroxyl group of one molecule acts as a proton donor and the chloride ion of the adjacent molecule acts as a proton acceptor. In the complex salt [H_2–Cn][$CoCl_4$] the Co···Co distance is shorter (7.024 Å) than in [(H–Cn)$CoCl_3$]·CH_3OH, but the contacts between the individual $[CoCl_4]^{2-}$ anions are accomplished through two hydrogen bonds, and the intermediate is a large organic cation, which is obviously not suitable for the intermolecular magnetic interactions between cobalt ions.

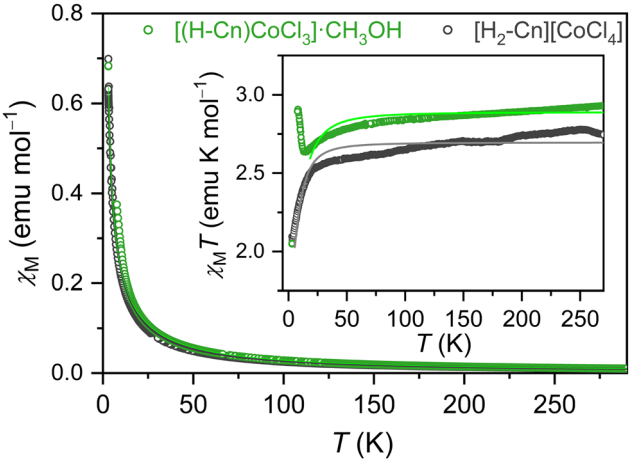

Fig. 6 Temperature dependence of the molar magnetic susceptibility (χ_M) of [(H–Cn)$CoCl_3$]·CH_3OH and [H_2–Cn][$CoCl_4$] (calculated for one Co atom) measured in a field of 1000 Oe. Inset shows the temperature dependence of the molar magnetic susceptibility and the temperature product ($\chi_M T$). The solid lines represent the corresponding fitting curves.

For both compounds, the susceptibility data in the temperature range of 14–290 K can be fitted in program PHI[37] assuming a simple zero-filed splitting effect, leading to values for the g-factor and the zero-field splitting term D, g = 2.482(1) and D = −4.52(4) cm^{-1} in [(H–Cn)$CoCl_3$]·CH_3OH and g = 2.397(1) and D = −9.7(1) cm^{-1} in [H_2–Cn][$CoCl_4$]. These values are in very good agreement with previously determined g and D values for cobalt(II) in similar environments.[38–41] A similar magnetic behaviour with a sharp low-temperature peak was

also observed in mononuclear cobalt(II) complexes with bis(imino)pyridine pincer ligands, which are single-molecule magnets according to the temperature and frequency dependent ac susceptibility measurements.[42] This is a clear indication that intermolecular interactions, in addition to affecting crystal packing, can lead to magnetic coupling of very distant metal centres mediated by hydrogen bonds.[43]

Chemoresistive sensing properties

Based on vacuum FTIR experiments, the compound [(H–Cn)$CoCl_3$] adsorbs methanol in the gas phase already at 25 ppm level. The reasons for such a rapid response to methanol molecules were explained by a detailed investigation of the structure of the compound [(H–Cn)$CoCl_3$], in particular the intermolecular interactions between the methanol and complex. The voids present in the structure of [(H–Cn)$CoCl_3$] are ideal for accommodating methanol molecules without significantly altering the volume of the unit cell itself. As vacuum FTIR measurements also showed that water molecules do not penetrate the structure of [(H–Cn)$CoCl_3$], this material proved to be highly specific and selective for the potential application of methanol detection. This is particularly important for methanol production, fuel processing, industrial monitoring and food packaging safety testing.[44] For the precise and quantitative detection of methanol gas, conventional active materials consisting mainly of metal oxide semiconductors and operating at high temperatures (above 400 K), such as SnO_2, are generally used. For the detection of methanol gas, metal–organic materials could offer certain advantages, such as operation at room temperature, selective detection in the sub-ppm range, chemical and structural tunability, and simple and environmentally friendly fabrication protocols.[44–46]

The sensing properties of pressed [(H–Cn)$CoCl_3$] and [H_2–Cn][$CoCl_4$] pellets were investigated by exposing the material to solvent vapours (methanol, acetonitrile and water) under atmospheric conditions (298 K, 1010 hPa, ~45% RH). For this purpose, gold electrodes were deposited on both surfaces of the pellet and the chronoamperometric current (at 10 V) was measured in Au/pellet/Au sandwich configuration. Fig. 7 shows that methanol vapour in the surrounding atmosphere strongly influences the electrical properties of [(H–Cn)$CoCl_3$].

After the addition of 100 ppm methanol, an increase in current of four orders of magnitude was observed, which is related to the diffusion of methanol molecules into the pellet and the uptake of methanol leading to a structural change to the methanol-solvent compound, the [(H–Cn)$CoCl_3$]·CH_3OH phase. The return to the initial phase after methanol exposure can be achieved by opening the chamber and releasing dry nitrogen gas into the system, which is registered by a drop in the current response in chronoamperometric measurements. The cycles of methanol exposure, *i.e.* the formation of the [(H–Cn)$CoCl_3$]·CH_3OH phase and the subsequent recovery to the [(H–Cn)$CoCl_3$] phase, are time-dependent. During the first cycle of methanol exposure in Fig. 7, it can be observed that a larger change in the current response is achieved with longer exposure and subsequent drying. Since the measurements are carried out on a pressed pellet with large, sputtered gold electrodes, the diffusion of molecules from the vapour phase is somewhat restricted by this geometry. In comparison, the dynamics of methanol uptake and desorption are much faster in thin films of this system,[22] which is related to the larger surface area of the films structured specifically for these resistive methanol sensing applications.

The ability of the complex salt [H_2–Cn][$CoCl_4$] to recognise the presence of solvent molecules was also tested. When solvent molecules are introduced into the closed chamber, they lead to an increase in the current flowing through the pressed pellet. The extent of the current change is different for acetonitrile, methanol and water (Fig. 8). For acetonitrile and methanol, a sharp drop in resistance is observed when nitrogen gas enters, which is accompanied by the complete removal of the solvent molecules, restoration of the [H_2–Cn][$CoCl_4$] phase and the complete reversibility of the behaviour. The release of water molecules by purging with nitrogen is not as rapid but the uptake is faster, which is consistent with other measurements (vacuum FTIR, TG and PXRD) showing that the water in the [H_2–Cn][$CoCl_4$]·H_2O phase is more strongly bound by intermolecular forces.

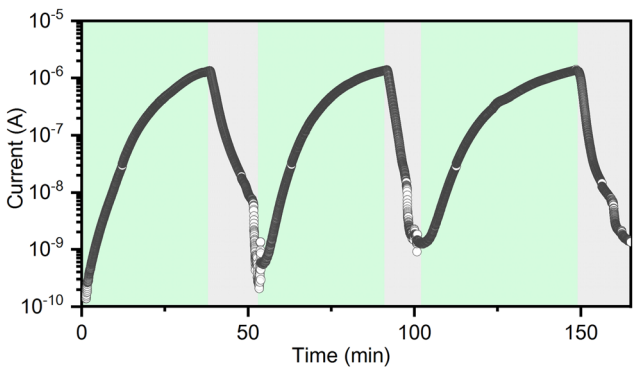

Fig. 7 Change in current response upon exposure to 100 ppm methanol vapours (green coloured area) and dry nitrogen (grey coloured area) of [(H–Cn)$CoCl_3$] at 298 K and ambient pressure.

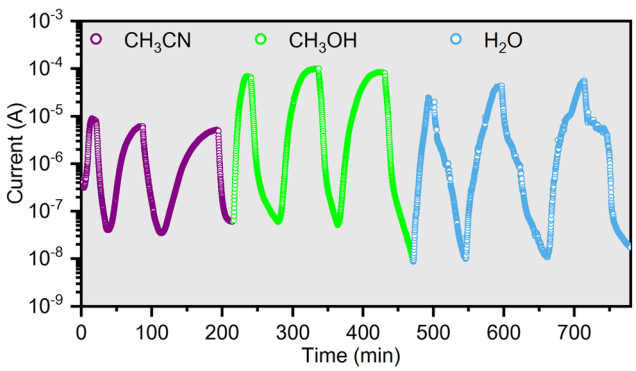

Fig. 8 Chemoresistive response of [H_2–Cn][$CoCl_4$] in the alternating presence of 100 ppm of various solvent vapours and dry nitrogen at 298 K and ambient pressure.

The observed effect of acetonitrile and methanol on the current increase is certainly related to the diffusion of the vapours of these solvents into the $[H_2–Cn][CoCl_4]$ pellet, which as polar molecules create conductive paths between the boundaries of the crystal grains. Although the structural changes of the $[H_2–Cn][CoCl_4]$ compound in the presence of methanol and acetonitrile were only observed during the mechanochemical reaction (and not by exposing the compound to these solvent vapours), future work will investigate whether the applied voltage of the chronoamerometric measurement nevertheless influences the change in the structure of the material in the presence of these solvent vapours.

Conclusion

The complex based on a natural alkaloid, the cinchoninium–trichloro–cobalt(II) complex $[(H–Cn)CoCl_3]$, proved to be a stimuli-responsive crystal which responds to environmental triggers with a change in structure and physicochemical properties. Exposure of $[(H–Cn)CoCl_3]$ to methanol vapours leads to reversible changes in the $[(H–Cn)CoCl_3]\cdot CH_3OH$ phase, with little intervention in volume and crystal packing. Furthermore, the compound showed such selectivity that water and acetonitrile do not enter the structure from the vapour, although water can be incorporated into the structure by a mechanochemically assisted reaction to form a hydrate phase $[(H–Cn)CoCl_3]\cdot H_2O$. Since the entry of methanol into $[(H–Cn)CoCl_3]$ is a low energy process, chronoamperometric measurements indicate that the material is suitable for methanol detection, with 25 ppm capable of complete structural conversion to $[(H–Cn)CoCl_3]\cdot CH_3OH$. Reconstructive solid-state transformations are triggered by corrosive HCl molecules that cause a transformation of the complex into the complex salt $[H_2–Cn][CoCl_4]$, which is accompanied by an increase in symmetry but a loss of polar order, from monoclinic $P2_1$ to orthorhombic $P2_12_12_1$. This structural change also has an effect on the magnetic properties, as the intermolecular interactions change significantly creating pathway to transmit magnetic coupling, especially at low temperatures, and in addition, a nitrogen atom is replaced by chlorine in the coordination sphere of the cobalt. Overall, it has been shown that small (solvent) molecules can influence changes in the structure and properties of metal–organic crystals, which is of interest for the design strategy of molecules-based materials that respond to stimuli with variable properties.

Conflicts of interest

There are no conflicts to declare.

Data availability

The data supporting this article are given in the SI.

Crystallographic details and geometry (Tables S1–S6, Fig. S1), FTIR spectra (Fig. S2–S4), TG data (Fig. S5, Table S7). See DOI: https://doi.org/10.1039/d5qi01084e.

CCDC 2444816–2444819 contain the supplementary crystallographic data for this paper.[47a–d]

Acknowledgements

Financial support from the Croatian Science Foundation (UIP-2019-04-7433) is gratefully acknowledged.

References

1 R. Torres-Cavanillas and A. Forment-Aliaga, Design of stimuli-responsive transition metal dichalcogenides, *Commun. Chem.*, 2024, **7**, 241.
2 T. Sun, R. Fan, J. Zhang, M. Qin, W. Chen, X. Jiang, K. Zhu, C. Ji, S. Hao and Y. Yang, Stimuli-Responsive Metal–Organic Framework on a Metal–Organic Framework Heterostructure for Efficient Antibiotic Detection and Anticounterfeiting, *ACS Appl. Mater. Interfaces*, 2021, **13**(30), 35689–35699.
3 W. Wu, K. Chen, T. Wang, N. Wang, X. Huang, L. Zhou, Z. Wang and H. Hao, Stimuli-responsive flexible organic crystals, *J. Mater. Chem. C*, 2023, **11**, 2026–2052.
4 K. Kaushik, S. Mehta, M. Das, S. Ghosh, S. Kamilya and A. Mondal, Stimuli-responsive magnetic materials: impact of spin and electronic modulation, *Chem. Commun.*, 2023, **59**, 13107–13124.
5 M. Kato, H. Ito, M. Hasegawa and K. Ishii, Soft Crystals: Flexible Response Systems with High Structural Order, *Chem. – Eur. J.*, 2019, **25**, 5105–5112.
6 Q. Guan, Y. Fang, X. Wu, R. Ou, X. Zhang, H. Xie, M. Tang and G. Zeng, Stimuli responsive metal organic framework materials towards advanced smart application, *Mater. Today*, 2023, **64**, 138–164.
7 L. Vanduyfhuys, S. M. J. Rogge, J. Wieme, S. Vandenbrande, G. Maurin, M. Waroquier and V. Van Speybroeck, Thermodynamic insight into stimuli-responsive behaviour of soft porous crystals, *Nat. Commun.*, 2018, **9**, 204.
8 M. Dunatov, A. Puškarić and L. Androš Dubraja, Multi-stimuli responsive (l-tartrato)oxovanadium(v) complex salt with ferroelectric switching and thermistor properties, *J. Mater. Chem. C*, 2023, **11**, 2880–2888.
9 L. Hu, Q. Zhang, X. Lic and M. J. Serpe, Stimuli-responsive polymers for sensing and actuation, *Mater. Horiz.*, 2019, **6**, 1774–1793.
10 D. Yan, Z. Wang and Z. Zhang, Stimuli-Responsive Crystalline Smart Materials: From Rational Design and Fabrication to Applications, *Acc. Chem. Res.*, 2022, **55**(7), 1047–1058.
11 X.-Y. Dong, Y. Si, J.-S. Yang, C. Zhang, Z. Han, P. Luo, Z.-Y. Wang, S.-Q. Zang and T. C. W. Mak, Ligand engineering to achieve enhanced ratiometric oxygen sensing in a

silver cluster-based metal-organic framework, *Nat. Commun.*, 2020, **11**, 3678.
12 H. He, L. Hashemi, M.-L. Hu and A. Morsali, The role of the counter-ion in metal-organic frameworks' chemistry and applications, *Coord. Chem. Rev.*, 2018, **376**, 319–347.
13 G. J. O. Beran, Frontiers of molecular crystal structure prediction for pharmaceuticals and functional organic materials, *Chem. Sci.*, 2023, **14**, 13290–13312.
14 O. Lagerna, A. Shivanyuk, G. A. Dolgonos, S. Shishkina, T. Kienko, A. Poyarkov, I. Tarchuk, O. Lukin and V. Fetyukhin, Towards Amplified Probing of Weak Intermolecular Interactions on the External Surfaces of Molecular Capsules, *Chem. – Eur. J.*, 2024, **30**, e202304006.
15 T. Phuong Thuy Hoang, C. Roullier, L. Evanno, I. Kerzaon, E. Gentil, T. Robiou du Pont, E.-H. Nazih, Y. F. Pouchus, S. Bertrand, E. Poupon and O. Grovel, Nature-Inspired Chemistry of Complex Alkaloids: Combining Targeted Molecular Networking Approach and Semisynthetic Strategy to Access Rare Communesins in a Marine-Derived Penicillium expansum, *Chem. – Eur. J.*, 2023, **29**, e202300103.
16 H. M. R. Hoffmann and J. Frackenpohl, Recent Advances in Cinchona Alkaloid Chemistry, *Eur. J. Org. Chem.*, 2004, **2004**(21), 4293–4312.
17 I. Hisaki, E. Hiraishi, T. Sasaki, H. Orita, S. Tsuzuki, N. Tohnai and M. Miyata, Crystal Structure of Quinine: The Effects of Vinyl and Methoxy Groups on Molecular Assemblies of Cinchona Alkaloids Cannot Be Ignored, *Chem. – Asian J.*, 2012, **7**, 2607–2614.
18 J. Achan, A. O. Talisuna, A. Erhart, A. Yeka, J. K. Tibenderana, F. N. Baliraine, P. J. Rosenthal and U. D'Alessandro, Quinine, an old anti-malarial drug in a modern world: role in the treatment of malaria, *Malar. J.*, 2011, **10**, 144.
19 S. Zheng, C. M. Schienebeck, W. Zhang, H.-Y. Wang and W. Tang, Cinchona Alkaloids as Organocatalysts in Enantioselective Halofunctionalization of Alkenes and Alkynes, *Asian J. Org. Chem.*, 2014, **3**, 366–376.
20 T. Kaczorowski, I. Justyniak, T. Lipínska, J. Lipkowski and J. Lewiński, Metal Complexes of Cinchonine as Chiral Building Blocks: A Strategy for the Construction of Nanotubular Architectures and Helical Coordination Polymers, *J. Am. Chem. Soc.*, 2009, **131**, 5393–5395.
21 H.-L. Cai, T. Zhang, L.-Z. Chen and R.-G. Xiong, The first homochiral compound with temperature-independence of piezoelectric properties, *J. Mater. Chem.*, 2010, **20**, 1868–1870.
22 M. Mesić and L. Androš Dubraja, Humidity modulated surface pattering of large-scale molecular ferroelectric thin films based on natural alkaloids, *Appl. Surf. Sci.*, 2025, **684**, 161841.
23 M. Očić and L. Androš Dubraja, Intermolecular Interactions in Molecular Ferroelectric Zinc Complexes of Cinchonine, *Crystals*, 2024, **14**, 978.
24 M. C. Burla, R. Caliandro, B. Carrozzini, G. L. Cascarano, C. Cuocci, C. Giacovazzo, M. Mallamo, A. Mazzone and G. Polidori, Crystal structure determination and refinement via SIR2014, *J. Appl. Crystallogr.*, 2015, **48**, 306–309.
25 G. M. Sheldrick, Crystal structure refinement with SHELXL, *Acta Crystallogr., Sect. C: Struct. Chem.*, 2015, **71**, 3–8.
26 L. J. Farrugia, WinGX and ORTEP for Windows: an update, *J. Appl. Crystallogr.*, 2012, **45**, 849–854.
27 A. L. Spek, Structure validation in chemical crystallography, *Acta Crystallogr., Sect. D: Biol. Crystallogr.*, 2009, **65**, 148–155.
28 F. Macrae, P. R. Edgington, P. McCabe, E. Pidcock, G. P. Shields, R. Taylor, M. Towler and J. van de Streek, Mercury: visualization and analysis of crystal structures, *J. Appl. Crystallogr.*, 2006, **39**, 453–457.
29 M. A. Thompson, QM/MMpol: A consistent model for solute/solvent polarization. Application to the aqueous solvation and spectroscopy of formaldehyde, acetaldehyde, and acetone, *J. Phys. Chem.*, 1996, **100**, 14492–14507.
30 G. S. Pawley, Unit-cell refinement from powder diffraction scans, *J. Appl. Crystallogr.*, 1981, **14**, 357–361.
31 V. A. Blatov, A. A. Golov, C. Yang, Q. Zeng and A. A. Kabanov, Network topological model of reconstructive solid-state transformations, *Sci. Rep.*, 2019, **9**, 6007.
32 A. Skórska, B. J. Oleksyn and J. Śliwínski, Cobalt Complex of Cinchonine: Intermolecular Interactions in Two Crystalline Modifications, *Enantiomer*, 2002, **7**, 295–303.
33 H. Myneni, E. Örn Jónsson, H. Jónsson and A. Ougaard Dohn, Polarizable Force Field for Acetonitrile Based on the Single-Center Multipole Expansion, *J. Phys. Chem. B*, 2022, **126**, 9339–9348.
34 K. Nakamoto, *Infrared and Raman Spectra of Inorganic and Coordination Compounds*, John Wiley, New York, 6th edn, 2009.
35 A. E. Özel, Y. Büyükmurat and S. Akyüz, Infrared-spectra and normal-coordinate analysis of quinoline and quinoline complexes, *J. Mol. Struct.*, 2001, **565–566**, 455–462.
36 M. Dunatov, K. Molčanov, Z. Štefanić, R. Kruk and L. Androš Dubraja, Interfacial Water Molecules as Agents for Phase Change Control and Proton Conductivity Enhancement in the Ammonium Vanadyl Tartrate System, *Inorg. Chem.*, 2024, **63**, 163–172.
37 N. F. Chilton, R. P. Anderson, L. D. Turner, A. Soncini and K. S. Murray, PHI: a powerful new program for the analysis of anisotropic monomeric and exchange-coupled polynuclear d- and f-block complexes, *J. Comput. Chem.*, 2013, **34**, 1164–1175.
38 A. Landart-Gereka, M. M. Quesada-Moreno, I. F. Díaz-Ortega, H. Nojiri, M. Ozerov, J. Krzystek, M. A. Palacios and E. Colacio, Large easy-axis magnetic anisotropy in a series of trigonal prismatic mononuclear cobalt(II) complexes with zero-field hidden single-molecule magnet behaviour: the important role of the distortion of the coordination sphere and intermolecular interactions in the slow relaxation, *Inorg. Chem. Front.*, 2022, **9**, 2810–2831.
39 O. Y. Vassilyeva, E. A. Buvaylo, V. N. Kokozay, B. W. Skelton, C. Rajnák, J. Titiš and R. Boča, Long magnetic relaxation time of tetracoordinate Co^{2+} in imidazo[1,5-a]pyridinium-

based $(C_{13}H_{12}N_3)_2[CoCl_4]$ hybrid salt and $[Co(C_{13}H_{12}N_3)Cl_3]$ molecular complex, *Dalton Trans.*, 2019, **48**, 11278–11284.

40 C. Belloso-Casuso, I. de Pedro, L. Canadillas-Delgado, G. Beobide, M. Sánchez-Andújar, J. Gárcia Ben, J. Walker, P. González Izquierdo, I. Cano, J. Rodríguez Fernández and O. Fabelo, Structural and physico-chemical characterization of hybrid materials based on globular quinuclidinium cation derivatives and tetrachloridocobaltate(ii) anions, *CrystEngComm*, 2024, **26**, 439–451.

41 M. A. Hay, A. Sarkar, G. A. Craig, L. Bhaskaran, J. Nehrkorn, M. Ozerov, K. E. R. Marriott, C. Wilson, G. Rajaraman, S. Hill and M. Murrie, In-depth investigation of large axial magnetic anisotropy in monometallic 3d complexes using frequency domain magnetic resonance and ab initio methods: a study of trigonal bipyramidal Co (II), *Chem. Sci.*, 2019, **10**, 6354–6361.

42 T. Jurca, A. Farghal, P.-H. Lin, I. Korobkov, M. Murugesu and D. S. Richeson, Single-molecule magnet behavior with a single metal center enhanced through peripheral ligand modifications, *J. Am. Chem. Soc.*, 2011, **133**, 15814–15817.

43 M. Atzori, A. Serpe, P. Deplano, J. A. Schlueter and M. L. Mercuri, Tailoring magnetic properties of molecular materials through non-covalent interactions, *Inorg. Chem. Front.*, 2015, **2**, 108–115.

44 F. Dai, X. Cui, Y. Luo, D. Zhang, N. Li, Y. Huang and Y. Peng, Ultrathin MOF nanosheet-based resistive sensors for highly sensitive detection of methanol, *Chem. Commun.*, 2022, **58**, 11543–115546.

45 M. S. Hosseini, S. Zeinali and M. H. Sheikhi, Fabrication of capacitive sensor based on Cu-BTC (MOF-199) nanoporous film for detection of ethanol and methanol vapors, *Sens. Actuators, B*, 2016, **230**, 9–16.

46 Z. Zhai, Y. Sun, X. Hao and C. Li, Capacitive gas sensors based on a ZIF-67/PAN nanofiber membrane to detect volatile organic compounds, *Appl. Surf. Sci.*, 2023, **621**, 156833.

47 (*a*) L. Androš Dubraja, CCDC 2444816: Experimental Crystal Structure Determination, 2025, DOI: **10.5517/ccdc.csd.cc2n211v**; (*b*) L. Androš Dubraja, CCDC 2444817: Experimental Crystal Structure Determination, 2025, DOI: **10.5517/ccdc.csd.cc2n212w**; (*c*) L. Androš Dubraja, CCDC 2444818: Experimental Crystal Structure Determination, 2025, DOI: **10.5517/ccdc.csd.cc2n213x**; (*d*) L. Androš Dubraja, CCDC 2444819: Experimental Crystal Structure Determination, 2025, DOI: **10.5517/ccdc.csd.cc2n214y**.